01 May 2023

A Hyperbaric Aerodynamic Levitator For Containerless Materials Research

Sydney E. Boland

Stephen K. Wilke

Jonathan A. Scott

Sarah M. Schlossberg

et. al. For a complete list of authors, see https://scholarsmine.mst.edu/matsci_eng_facwork/2947

Recommended Citation

S. E. Boland et al., "A Hyperbaric Aerodynamic Levitator For Containerless Materials Research," *Review of Scientific Instruments*, vol. 94, no. 5, article no. 053903, American Institute of Physics, May 2023.
The definitive version is available at https://doi.org/10.1063/5.0148455

Review of Scientific Instruments

RESEARCH ARTICLE | MAY 19 2023

A hyperbaric aerodynamic levitator for containerless materials research

Sydney E. Boland ; Stephen K. Wilke ; Jonathan A. Scott ; Sarah M. Schlossberg ; Alex Ivaschenko ; Richard J. K. Weber ; David W. Lipke

Rev Sci Instrum 94, 053903 (2023)
https://doi.org/10.1063/5.0148455

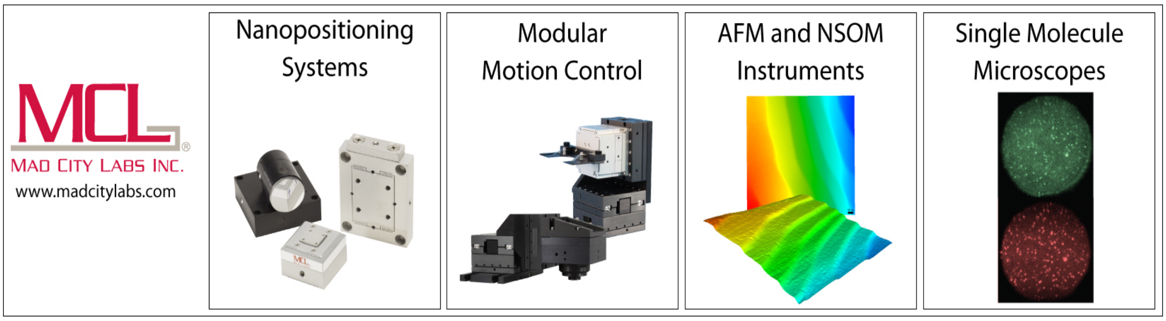

AIP Publishing

Review of Scientific Instruments | ARTICLE | scitation.org/journal/rsi

A hyperbaric aerodynamic levitator for containerless materials research

Cite as: Rev. Sci. Instrum. 94, 053903 (2023); doi: 10.1063/5.0148455
Submitted: 1 March 2023 • Accepted: 5 May 2023 •
Published Online: 19 May 2023

Sydney E. Boland,[1] Stephen K. Wilke,[2] Jonathan A. Scott,[1] Sarah M. Schlossberg,[2] Alex Ivaschenko,[3] Richard J. K. Weber,[2] and David W. Lipke[1,a)]

AFFILIATIONS

[1] Department of Materials Science and Engineering, Missouri University of Science and Technology, Rolla, Missouri 65409, USA
[2] Materials Development, Inc., Arlington Heights, Illinois 60004, USA
[3] Encole LLC, San Jose, California 95134, USA

[a)] Author to whom correspondence should be addressed: Lipke@mst.edu

ABSTRACT

A hyperbaric aerodynamic levitator has been developed for containerless materials research at specimen temperatures exceeding 2000 °C and pressures up to 10.3 MPa (1500 psi). This report describes the prototype instrument design and observations of the influence of specimen size, density, pressure, and flow rate on levitation behavior. The effect of pressure on heat transfer was also assessed by studying the heating and cooling behavior of levitated Al_2O_3 liquids. A threefold increase in the convective heat transfer coefficient was estimated as pressure increased to 10.3 MPa. The results demonstrate that hyperbaric aerodynamic levitation is a promising technique for containerless materials research at high gas pressures.

I. INTRODUCTION

Levitators are useful for studying solidification and vitrification phenomena of ubiquitous importance to materials that undergo solid-liquid phase transitions during their natural history or in industrial processing, and, consequently, levitators boast a strong legacy of materials discovery breakthroughs.[1–4] Researchers have used levitators to synthesize and study some of the earliest known examples of ultra-high purity semiconductors[5,6] and bulk metallic glasses.[7] Levitators have enabled advances in fundamental science by providing direct evidence of liquid–liquid phase transitions[8–11] and by elucidating the high temperature structural chemistry of corrosive and hazardous materials.[12,13] Levitators serve as sample environments for synchrotron beamlines for the acquisition of atomic structure data while simultaneously probing structural chemistry via high energy x-ray scattering techniques.[3,14–20]

Levitators can attain specimen temperatures of 2000 °C or greater using directed energy sources such as lasers, including continuous wave CO_2 lasers (CW CO_2), electron beams, electromagnetic inductive coupling, or combinations thereof. Ambient environments in standard levitators vary from high vacuum to near-atmospheric pressures depending on the requirements of the selected levitation and heating methods and instrument design limitations. For example, maintaining surface charge on electrostatically levitated specimens normally requires the use of vacuum environments, making the technique incompatible with use at elevated pressures. Other levitation techniques, such as electromagnetic levitation, acoustic levitation, and aerodynamic levitation, do not share this intrinsic incompatibility, though instrument designs supporting high pressure operation have not been widely available. However, a small number of special purpose levitators capable of hyperbaric operation (i.e., operating at greater than normal atmospheric pressure) have been reported, as summarized in Table I.

Hyperbaric levitators employing the acoustic principle of levitation are limited by the maximum operating transducer temperature, restricting their use to low-to-intermediate specimen temperatures (as in the cases of the chamber heating design[22] and prototype laser-heated acoustic levitator[21]) or to short heating durations (as in the case of the pulsed laser-heated design[23,24]). Pulse-heating techniques can attain extreme specimen temperatures, although short (ms) heating times limit the types of measurements that can be made. Hyperbaric levitators employing other techniques such as buoyant levitation or electromagnetic levitation are inherently limited by specimen properties, being restricted to specimens having

TABLE I. Overview of hyperbaric levitators used for containerless materials research.

Principle of levitation	Heating source	Max. specimen temperature (°C)	Max. operating pressure (MPa)	References
Acoustic	Laser (CW CO_2)	1300	0.9	21
Acoustic	Jacketed chamber	180	20	22
Acoustic	Laser (pulsed CO_2)	5000	30	23 and 24
Aerodynamic	Laser (CW CO_2)	2200	10.3	This work
Hybrid aerodynamic electrostatic	Laser (CW CO_2)	2000	1	17 and 25
Buoyant	Radiant heater (HIP)	1800	200	26
Electrostatic	Laser (CW CO_2)	2700	0.3	27
Electromagnetic	Induction	1600	10	28
Electromagnetic	Induction	1900	5	29

low densities or high electrical conductivities, respectively. The principle of aerodynamic levitation is not inherently limited by specimen properties and is theoretically compatible with pressurized environments, although hyperbaric aerodynamic levitators capable of operation at pressures much above 1 MPa (10 bars) have not been demonstrated prior to this work.[4,17,25]

Containerless experimentation at high gas pressures confers two primary benefits. First, pressurized systems are known to suppress volatilization. For example, when limited by mass transport through an external boundary layer, evaporation rates are proportional to $1/\sqrt{P}$ up to a critical pressure on the order of 1–100 MPa.[30,31] With reduced volatile losses, specimen composition can be better preserved. Specimens may also be observed for longer durations, enabling measurements of the properties and/or structural chemistry of highly volatile materials. Second, reactive gas pressures possess increased chemical potentials $\Delta\mu_i = RT \ln f_i/f_i^\circ$, where i is a reactive species (e.g., oxygen or nitrogen) whose magnitude may attain ~100 kJ/mol at elevated temperatures. This increase in chemical potential can dramatically affect phase equilibria, a fact that has been exploited to synthesize new compounds using elevated pressure crystal growth, surface heating, and/or melting.[32–42]

This work describes the design and performance characteristics of a prototype hyperbaric aerodynamic levitator for containerless materials research. The levitation behaviors of two series of spherical specimens of varying sizes and densities were studied as functions of pressure and flow rate. Additionally, the effect of pressure on heat transfer was assessed by comparing the heating and cooling behaviors of levitated liquid Al_2O_3 at pressures up to 10.3 MPa.

II. INSTRUMENT DESCRIPTION

The hyperbaric aerodynamic levitator shown in Fig. 1 comprises four major components: a pressure vessel; a diamond window for CO_2 laser admittance; a converging-diverging conical nozzle; and pressurized fluid handling systems. System components and controls were carefully engineered for safe operation. The pressure vessel (Encole LLC, San Jose, CA, USA) consists of a machined billet of 7075-T6 aluminum featuring a vertical through-bore, multiple ports, and internal water-cooling passages. Finite element simulations were conducted to design the pressure vessel for a maximum internal pressure of 17.2 MPa (2500 psi) with a safety factor of four. A pressure-relief valve and burst disk were installed on the outlet and inlet sides of the pressure vessel, respectively. As an additional engineering control, operators were in a separate room from the hyperbaric levitator. The electronic backpressure regulator and mass flow controllers were operated via a computer interface with remote displays.

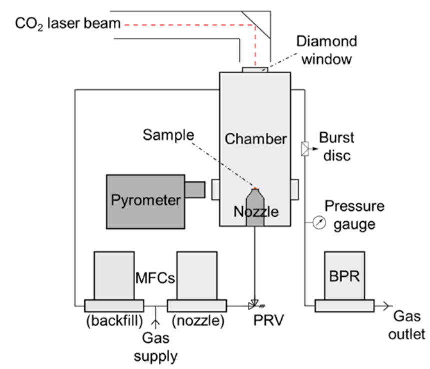

FIG. 1. Schematic of prototype hyperbaric aerodynamic levitator integrated with a CO_2 laser. Abbreviations: mass flow controllers (MFCs), back pressure regulator (BPR), pressure relief valve (PRV).

The converging-diverging levitation nozzle features conical semi-angles of 30°–60° intersecting at a cylindrical orifice whose diameter may vary from 0.5 to 2 mm.[20] The nozzle was vertically installed and sealed onto the pressure vessel with an SAE thread identical to that used for the sight glasses. The shallow conical nozzle design allowed for about half of the levitated specimen volume to be visible above the top of the nozzle as viewed from the horizontal sight glasses. During levitation experiments, the specimen was remotely viewed via a camera (acA150-uc, Basler) equipped with a 1.0X f/6-f/25 telecentric lens (Edmund Optics, Inc.) using a white LED backlight. The optical configuration provided a spatial resolution of 4.8 × 4.8 μm^2/pixel, and videos were recorded with a frame rate of 150 fps. Levitation stability, as indicated by the vertical displacement of the top of the sphere, was measured using motion tracking software (ProAnalyst, Xcitex Inc.).

A pair of mass flow controllers (SLA5850 Series, Brooks Instrument) independently provided pressurized fluid to the levitation nozzle (maximum volumetric flow rate Q = 5.0 standard liters per minute or SLM) and as a purge flow across the diamond window to abate deposit formation (max. Q = 0.5 SLM). Pressure within the chamber was controlled using an electronic backpressure regulator (SLA5820 Series, Brooks Instrument) located downstream of the pressure vessel outlet. During a typical levitation experiment, the purge flow was maintained at a constant 0.5 SLM until the system attained the ambient pressure setpoint. Flow through the conical nozzle was then increased until the maximum flow rate was attained or instabilities in the specimen position presenting as a lateral movement were observed. Subsequently, levitation height was recorded at different flow rates stepping down in increments of 0.1 SLM until the sphere no longer displayed stable levitation. In this investigation, two series of levitation experiments were conducted: aluminum spheres of varying diameter (2.529, 3.048, 3.575, or 3.979 mm) and 3 mm diameter spheres made from materials of varying density [aluminum: 2.71 g/cm^3, alumina (Al_2O_3): 3.95 g/cm^3, yttria-stabilized zirconia (YSZ): 6.00 g/cm^3, or type 302 stainless steel (SS302): 7.93 g/cm^3].

A custom sight glass featuring a 1.3 mm thick × 10 mm clear aperture diamond window (Element Six Technologies, Santa Clara, CA, USA) encased in an SAE-12 fitting made from 17-4PH steel (Encole, LLC). All sight glass housings featured SAE threads coated with WS_2 in accordance with AMS2530 to prevent galling during frequent disassembly. The diamond window provides excellent transmission for the 10.6 μm wavelength CW CO_2 laser (400 W Synrad Firestar i401, Novanta Photonics) used as a heating source in these studies. Diamond is an ideal material for this purpose, given its excellent thermal conductivity and high strength as compared to traditional CO_2 laser window materials such as ZnSe. In this work, the diamond window was uncoated; consequently, approximately one-third of incident laser energy was lost due to Fresnel reflections (i.e., diamond has an index of refraction of 2.376 at 10.6 μm).

III. HYPERBARIC AERODYNAMIC LEVITATION

Figure 2 shows the effect of volumetric flow rate Q on the stable levitation height of the specimen Z normalized to its diameter d at selected absolute pressures of 3.45 MPa (corresponding to a nitrogen density of 55.5 kg/m^3) and 10.3 MPa (corresponding to a nitrogen density of 166.6 kg/m^3). From the available data, it is recognized that Z/d increases with Q (at a fixed pressure and specimen density) and decreases with specimen density (at a fixed pressure and flow rate). Deviations from these trends are discernible. For example, an increase in Z/d when Q approaches 3.0 SLM at 10.3 MPa is observed for the 2.529, 3.048, and 3.575 mm diameter aluminum spheres that is not seen for the larger diameter aluminum spheres. Similarly, an increase in Z/d when Q approaches 3.0 SLM at 10.3 MPa is observed for the 3.000 mm diameter aluminum sphere, but not for this same sphere at 3.45 MPa or for 3.000 mm diameter spheres made from denser materials at either pressure. These results suggest that a change in drag force occurs across this flow rate regime whose magnitude is sufficient to displace the stable levitation position of relatively lightweight specimens.

To better understand observed trends, fluid mechanics relations were used to calculate drag force for varying experimental conditions. A necessary condition for aerodynamic levitation is given by the force balance,

$$\sum F_z = 0 = F_d + F_{\nabla P} + F_b - F_g \cong F_d - F_w, \tag{1}$$

where F_d is the drag force, $F_{\nabla P}$ is the pressure gradient force, F_b is the buoyant force, F_g is the force of gravity, and $F_w = F_g - F_b$ is the buoyant weight of the sphere. The buoyant weight must, therefore, be offset by the sum of the drag force and pressure gradient force. For clarity, herein, we neglect the pressure gradient force, as it is assumed the full pressure drop of the fluid jet occurs within the nozzle orifice (a detailed simulation would be needed to confirm this assumption).

The buoyant weight of a spherical specimen can be expressed in terms of specimen size (d), specimen density (ρ_s), fluid density (ρ), and acceleration due to gravity (g) as

$$F_w = \frac{1}{6}\pi d^3(\rho_s - \rho)g. \tag{2}$$

The drag force can be expressed as the product of the drag coefficient C_d, specimen area, and dynamic pressure,

$$F_d = C_d \cdot \frac{1}{2}\rho\left(\frac{\pi d^2}{4}\right)v^2. \tag{3}$$

In Eq. (3), velocity v is not singularly valued but rather varies with axial position as the flow diverges from the conical nozzle exit. The axial flow velocity can be taken to be inversely proportional to the vertical distance from the jet source,[43] or

$$v^2 = \left(\frac{A}{Z}\right)^2, \tag{4}$$

where A is a constant of dimensions length × velocity. Substitution of (4) into (3) yields

$$F_d = C_d \cdot \frac{1}{8}\pi\rho\frac{A^2}{\left(\frac{Z}{d}\right)^2}. \tag{5}$$

The constant A can be determined by the conservation of momentum flux by assuming the jet momentum J crossing any longitudinal surface located at a distance Z away from the jet source is constant. The jet momentum at the nozzle exit, J_{nozzle}, is, therefore, related to the constant A by the expression[43]

$$J_{nozzle} = \frac{1}{2}\rho\left(\frac{\pi D^2}{4}\right)v_{nozzle}^2 = \pi\rho A^2\beta^2, \tag{6}$$

where β is the cone angle of the jet, here assumed to be the same as the nozzle, and D is the diameter of the nozzle orifice. Re-arranging, the constant A is given by

$$A^2 = \frac{v_{nozzle}^2 D^2}{8\beta^2}. \tag{7}$$

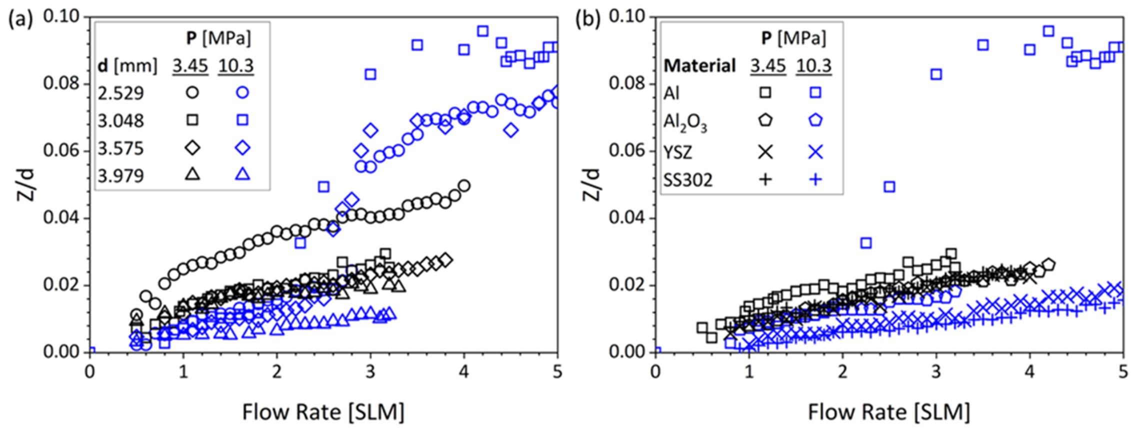

FIG. 2. Relative stable levitation position (Z/d) vs volumetric flow rate (SLM) for experimental series varying (a) diameter for Al specimens and (b) material [aluminum: 2.71 g/cm^3, alumina (Al_2O_3): 3.95 g/cm^3, yttria-stabilized zirconia (YSZ): 6.00 g/cm^3, or type 302 stainless steel (SS302): 7.93 g/cm^3] for 3.000 mm diameter spheres.

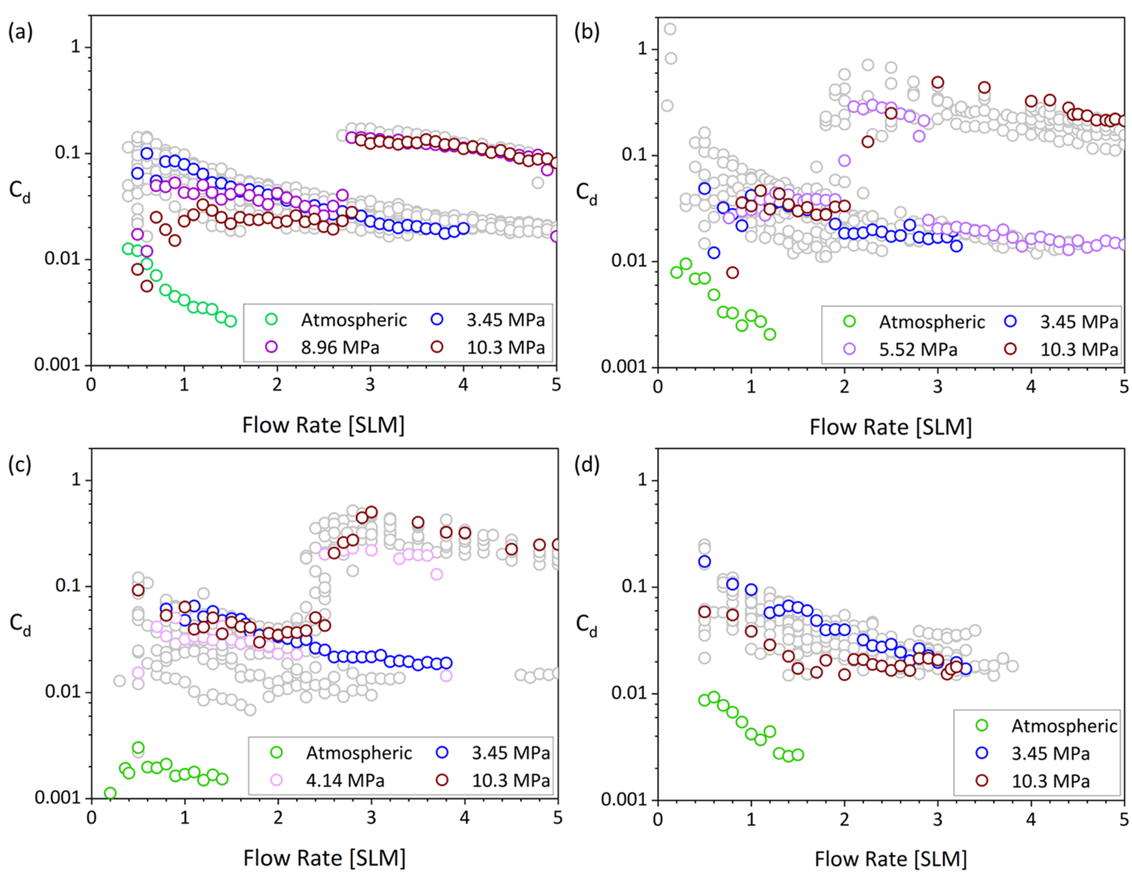

FIG. 3. Computed drag coefficients for Al specimens with diameters of (a) 2.529 mm, (b) 3.048 mm, (c) 3.575 mm, and (d) 3.979 mm as a function of volumetric flow rate.

The nozzle velocity can be expressed in terms of the experimental parameters of volumetric flow rate (Q), fluid density, and nozzle cross-sectional area,

$$v_{nozzle} = \frac{Q}{\rho\left(\frac{\pi D^2}{4}\right)}. \tag{8}$$

Substitution of (8) into (7) yields

$$A^2 = \frac{2Q^2}{\pi^2\rho^2 D^2\beta^2}. \tag{9}$$

Finally, substitution of (9) into (5) and equating to (2) yields the following expression for drag coefficient upon simplification and re-arrangement:

$$C_d = \frac{2\pi^2\left(\frac{Z}{d}\right)^2 d^3(\rho_s - \rho)g\rho D^2\beta^2}{3Q^2}. \tag{10}$$

Evaluating expression (10) using observed relative levitation heights as functions of flow rate and fluid density (i.e., pressure) yields computed drag coefficient values as shown in Figs. 3 and 4.

Figures 3 and 4 illustrate the occurrence of two drag coefficient regimes: a primary trendline onto which most observations fall and a secondary trendline that reflects the change in relative levitation height for lightweight samples (i.e., small size and/or low density) at moderate flow rates and high pressures. Highlighted pressure series correspond to the minimum and maximum pressures employed in this work, a selected common trend for comparison, and, where applicable, the pressure at which deviation in the trends first appears, while additional measured data series are grayed out for the sake of clarity. For example, Fig. 3(a) shows a jump in computed C_d values near 3.0 SLM for pressures exceeding 8.96 MPa. Observations fall on secondary trendlines for similar flow rates starting at pressures of 5.52 and 4.14 MPa, as shown respectively in Figs. 3(b) and 3(c), with increasing specimen diameter. The transitional nature of these drag coefficient regimes is captured in the highlighted pressure series at 5.52 MPa in Figs. 3(b) and 3(c), where the calculated C_d deviates from the primary trendline up to the secondary trendline before returning to the primary trendline at higher flow rates.

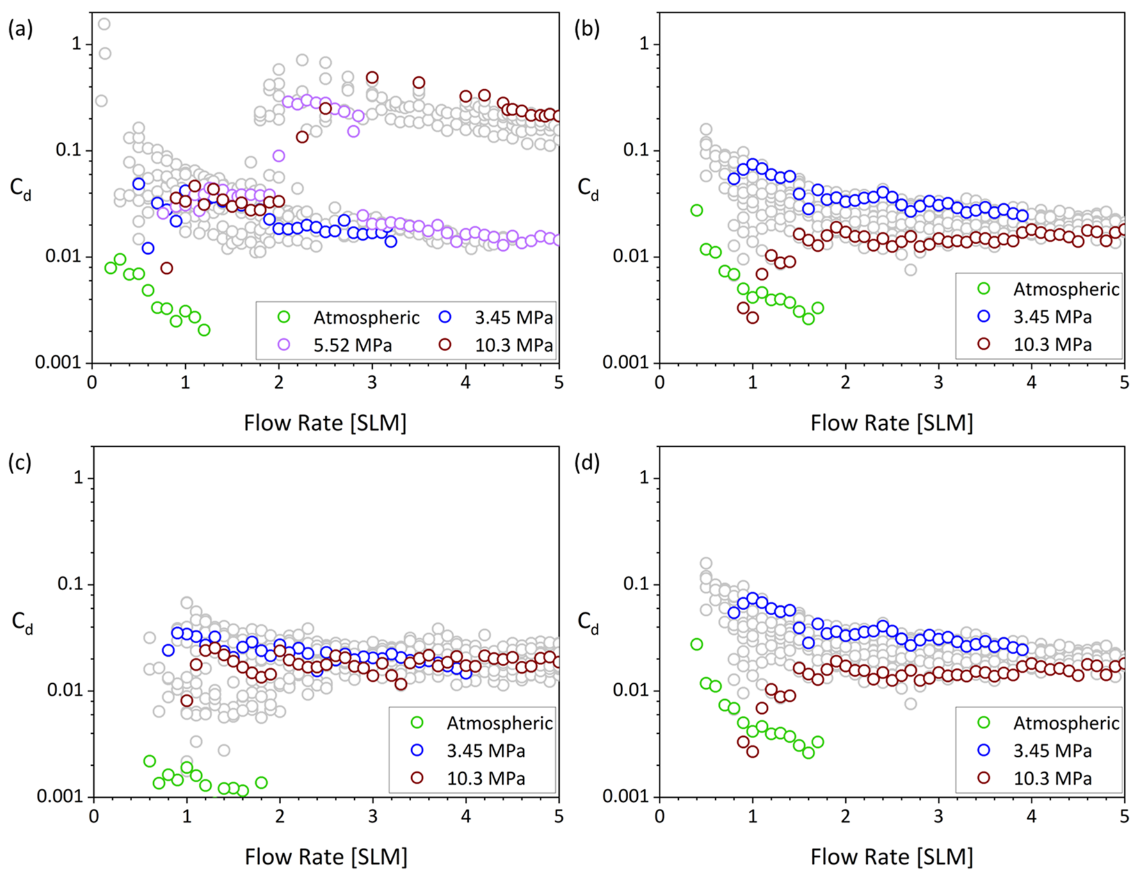

FIG. 4. Computed drag coefficients for 3.000 mm diameter Al specimens made from (a) Al, (b) Al_2O_3, (c) YSZ, and (d) SS302 as a function of volumetric flow rate.

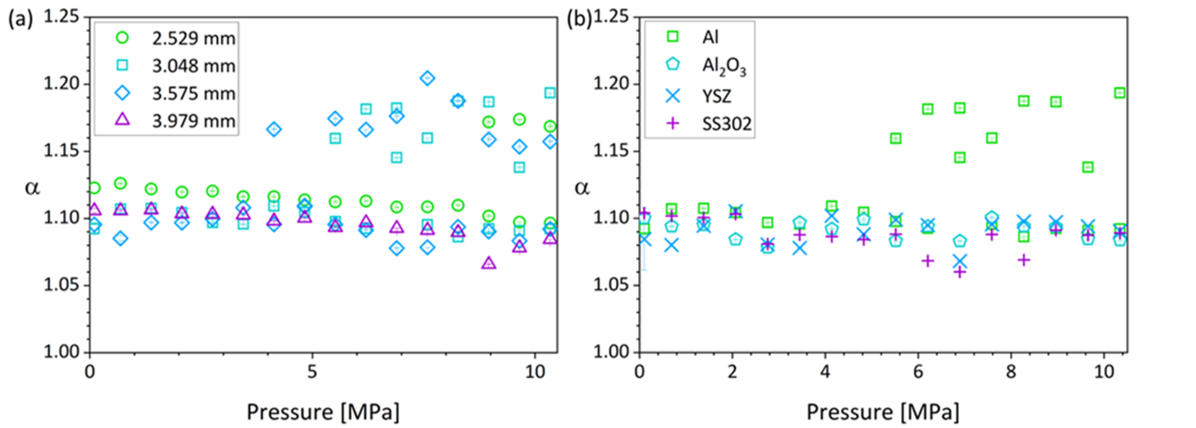

FIG. 5. Best fit α values for trends illustrated in Figs. 3 and 4 for the varying specimen (a) size and (b) material at pressures ranging from atmospheric to 10.3 MPa.

An alternative means to identify the onset of the secondary trendline employs a semi-empirical dimensionless scaling relation to describe the suspension of spheres in turbulent jets,

$$\left(\frac{C_d}{3}\right)^{1/2} Fr\left(\frac{\rho_s}{\rho}\right)^{-1/2}\left(\frac{d}{D}\right)^{-3/2} = \left(\frac{Z}{D}\right)^{1/\alpha}, \tag{11}$$

where Fr is the Froude number ($Fr = v/\sqrt{Dg}$).[44,45] This expression was used to numerically fit the free parameter α using the data from Figs. 3 and 4, as summarized in Fig. 5:

As shown in Fig. 5, the secondary trendline for lightweight specimens features a statistically different exponential dependence on experimental parameters as compared to the primary trendline. The origin of this difference is not well understood but is speculated to relate to wake turbulence transitions like those reported for spheres in comparable Reynolds and Froude number regimes.[46]

The effect of fluid density was also evaluated by comparing hyperbaric aerodynamic levitation behavior in nitrogen vs argon as a function of pressure. Figure 6 illustrates the levitation of 3.000 mm Al_2O_3 spheres at 3.45 MPa (Ar: 55.5 kg/m^3, N_2: 39.8 kg/m^3) and 10.3 MPa (Ar: 166.6 kg/m^3, N_2: 118.7 kg/m^3). At each pressure, the heavier fluid imparts more momentum to the sphere, resulting in a higher relative levitation height. As pressure increases and, consequently, flow velocity decreases at any given flow rate, relative levitation heights decrease for both fluids.

IV. HEAT TRANSFER IN DENSE FLUIDIZING MEDIA

A levitated 3.000 mm Al_2O_3 sphere was melted with a 400 W CO_2 laser at atmospheric pressure, 2.07, 4.14, 6.21, 8.27, and 10.3 MPa nitrogen to assess the effect of pressure on heat transfer characteristics. Levitation trials were conducted with a constant volumetric flow rate of 1.5 SLM at ambient pressures up to 4.14 MPa and a constant volumetric flow rate of 3.5 SLM for ambient pressures from 6.21 to 10.3 MPa, with flow rates selected to maximize specimen stability during heating.

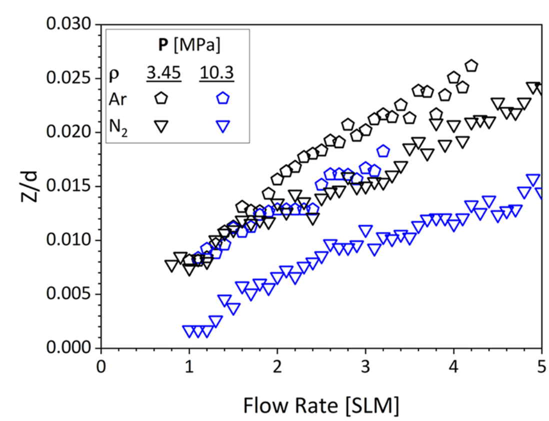

FIG. 6. Relative stable levitation height vs volumetric flow rate for a 3.000 mm Al_2O_3 sphere using argon or nitrogen as levitation fluid at selected pressures of 3.45 and 10.3 MPa.

Figure 7 shows the molten Al_2O_3 sphere levitated at atmospheric pressure and 10.3 MPa. At elevated pressures, the increased fluid density apparently leads to a concomitant change in the fluid refractive index, thereby allowing the turbulent flow structure to be visualized. Figure 8 shows cooling curves for the 3.000 mm Al_2O_3 sphere as measured by optical pyrometry (IR-CAS, Chino Corp.). Reported apparent temperatures are uncorrected for effects of view factor, specimen emissivity, or window absorption.

Convective heat transfer coefficients h were calculated from cooling curve data by fitting the following convection-radiation heat equation:

$$\rho_s c_p\left(\frac{\pi d^3}{6}\right)\frac{dT}{dt} + \pi d^2\left[h(T - T_\infty) + \varepsilon\sigma\left(T^4 - T_\infty^4\right)\right] = 0. \tag{12}$$

Calculations assumed a specimen emissivity of ε = 0.9, a constant sample density, and utilized reported literature values for

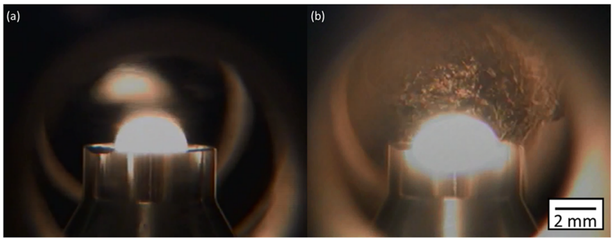

FIG. 7. Aerodynamically levitated molten Al_2O_3 droplet (initially a 3.000 mm diameter sphere) at (a) atmospheric pressure and (Multimedia available online). (b) at 10.3 MPa. At atmospheric pressure, a reflection of the sample on a window surface is clearly visible. At high pressure, strong convection results in a turbulent wake pattern in the fluid above the hot sample as well as blurring of the image (Multimedia available online).

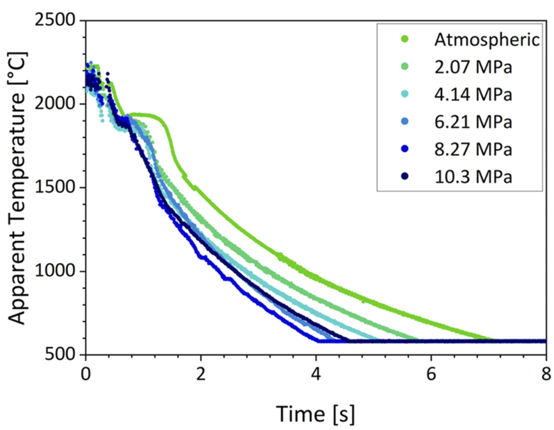

FIG. 8. Cooling curves of levitated Al_2O_3 liquids as recorded by optical pyrometry as a function of nitrogen pressure.

temperature-dependent heat capacity. The resulting values are summarized in Table II, where the convective heat transfer coefficient is shown to increase threefold as pressure increased from atmospheric pressure to 10.3 MPa.

The convective-radiative heat balance can be used to estimate the maximum attainable specimen temperatures as a function of absorbed laser energy and specimen surface area. Figure 9 shows calculated equilibrium temperatures using estimated heat transfer coefficients for atmospheric pressure aerodynamic levitation

TABLE II. Convective heat transfer coefficient calculated from cooling curve data for a 3.000 mm Al_2O_3 sphere at varying MPa pressures.

Pressure (MPa)	h (W/m^2 K)
Atmospheric	300 ± 200
2.07	500 ± 300
4.14	500 ± 200
6.21	700 ± 200
8.27	700 ± 200
10.3	900 ± 200

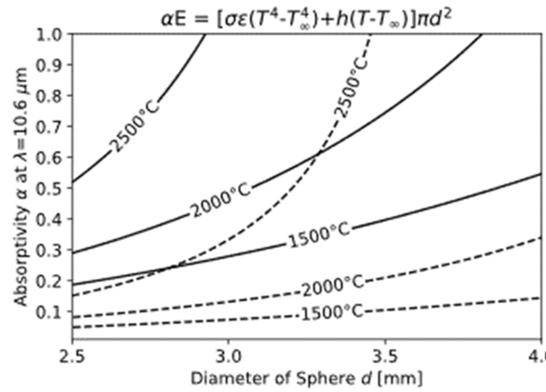

FIG. 9. Calculated equilibrium temperature vs specimen size using the heat balance equation shown. *E* is the output laser power (150 W) and *h* is the convective heat transfer coefficient (solid lines: 900 W/m^2 K, dashed lines: 300 W/m^2 K).

(dashed) and hyperbaric aerodynamic levitation (solid). Assuming a constant 150 W output laser power and a total hemispherical emissivity of 0.9, specimen temperatures above 2100 °C should be attainable for 3.0 mm specimens with absorptivity values greater than 0.6 at 10.6 μm. To attain higher specimen temperatures, additional laser energy must be delivered to the sample, which can likely be achieved via a combination of optimization of beam delivery optics, the use of anti-reflective coatings on the diamond window used for laser admittance, or increasing output laser power.

Concordant with increased convective heat losses, the additional laser power was required to melt the specimen. Figure 10 compares the laser power necessary to overcome convective heat losses for atmospheric pressure aerodynamic levitation vs hyperbaric aerodynamic levitation at 10.3 MPa by plotting measured apparent temperatures sampled every 62 ms as laser power was continuously increased until melting was attained. An increase of ~15% of the maximum laser power, corresponding to an additional 60 W, was required to attain molten Al_2O_3 at 10.3 MPa. This represents a modest increase relative to the total laser power

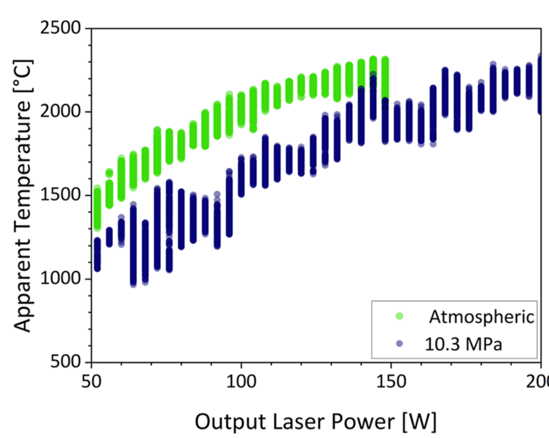

FIG. 10. Apparent temperature vs output laser power necessary to attain melting of a 3.000 mm Al_2O_3 sphere in nitrogen at atmospheric pressure and at 10.3 MPa.

available, indicating that materials with even greater melting points than Al_2O_3 can be levitation melted in hyperbaric conditions (note: as temperatures increase further above 2000 °C, radiative heat losses are expected to dominate over convective heat losses, such that increased convective heat losses at elevated pressures may become negligible).

V. CONCLUSIONS

A hyperbaric aerodynamic levitator for containerless materials research has been designed and tested. The instrument operates at ambient pressures up to 10.3 MPa and can attain specimen temperatures greater than 2100 °C, depending on material characteristics. Preliminary evaluations of hyperbaric aerodynamic levitation phenomena indicate stable levitation can be attained across a wide range of flow rates and pressures. For the nozzle configuration tested, two stable levitation regimes were observed for lightweight specimens that are speculated to be associated with a change in turbulent wake structure. Additional simulation and experimentation are recommended to better understand the effects of flow turbulence on levitation stability.

Output laser power necessary to melt specimens at elevated pressures increased due to enhanced convective heat transfer with increasing fluid density; however, the magnitude was modest—~60 W additional output laser power in going from atmospheric pressure to 10.3 MPa flowing nitrogen necessary to melt a 3.000 mm Al_2O_3 sphere. The results demonstrate that hyperbaric aerodynamic levitation is a promising technique for containerless materials research at high gas pressures.

The continued development of hyperbaric aerodynamic levitation is anticipated to enable previously unfeasible experiments. Future levitator designs compatible with high energy x-ray synchrotron beamlines will support *in situ* measurements of the structural chemistry of materials that would otherwise vaporize too quickly at high temperatures under atmospheric pressure. By suppressing volatilization rates, hyperbaric levitation may better preserve the complex chemistry of technologically important multicomponent systems, such as high entropy materials. Levitation under high reactive gas pressures also creates the possibility of extended redox regimes that may find applications in network glasses and functional ceramics whose properties are sensitive to oxidation states and point defect populations.

ACKNOWLEDGMENTS

The authors gratefully acknowledge the partial financial support for author Sydney E. Boland from the Office of Naval Research (ONR) Naval Engineering Education Consortium (NEEC) Grant No. N00174-21-1-0008. Funding assistance from the College of Engineering and Computing and the Materials Research Center at Missouri University of Science and Technology is gratefully acknowledged. The authors acknowledge the contributions of undergraduate students Brennan Long (Missouri S&T) and Gerald Amory (Morgan State University) for their assistance in early instrument development. We also extend sincere acknowledgment to Professor Mario Affatigato (Coe College) for assistance with prototype testing and stimulating discussions.

AUTHOR DECLARATIONS

Conflict of Interest

S.W. and R.W. disclose financial interests in Materials Development, Inc., a company involved in developing and selling levitation instruments.

Author Contributions

Sydney E. Boland: Formal analysis (lead); Investigation (lead); Methodology (equal); Validation (lead); Visualization (lead); Writing – original draft (lead); Writing – review & editing (equal). **Stephen K. Wilke**: Investigation (supporting); Methodology (equal); Visualization (supporting); Writing – review & editing (equal). **Jonathan A. Scott**: Methodology (equal). **Sarah M. Schlossberg**: Investigation (supporting); Visualization (supporting). **Alex Ivaschenko**: Resources (equal); Writing – review & editing (equal). **Richard J. K. Weber**: Funding acquisition (supporting); Investigation (supporting); Methodology (equal); Resources (equal); Supervision (equal); Writing – review & editing (equal). **David W. Lipke**: Conceptualization (lead); Funding acquisition (lead); Methodology (equal); Project administration (lead); Supervision (equal); Writing – review & editing (equal).

DATA AVAILABILITY

The data that support the findings of this study are available from the corresponding author upon reasonable request.

NOMENCLATURE

A	momentum flux constant
C_d	drag coefficient
c_p	heat capacity
D	diameter of nozzle
d	diameter of sphere
Fr	Froude number
g	standard acceleration due to gravity
h	convective heat transfer coefficient
Q	volumetric flow rate
v	velocity
Z/d	relative levitation height
β	cone angle of the nozzle
ε	emissivity
ρ	density of fluid
ρ_s	density of sphere
σ	Stefan–Boltzmann constant

REFERENCES

[1] E. H. Brandt, Science **243**, 349 (1989).
[2] M. Barmatz, MRS Online Proc. Libr. **9**, 25 (1981).
[3] D. M. Herlach, R. F. Cochrane, I. Egry, H. J. Fecht, and A. L. Greer, Int. Mater. Rev. **38**, 273 (1993).
[4] R. Weber, S. K. Wilke, and C. J. Benmore, J. Phys. Soc. Jpn. **91**, 091008 (2022).
[5] E. C. Okress, D. M. Wroughton, G. Comenetz, P. H. Brace, and J. C. R. Kelly, J. Appl. Phys. **23**, 545 (1952).
[6] G. R. Davies, Metall. Rev. **10**, 173 (1965).

[7] W. K. Rhim, S. K. Chung, D. Barber, K. F. Man, G. Gutt, A. Rulison, and R. E. Spjut, Rev. Sci. Instrum. **64**, 2961 (1993).
[8] P. F. McMillan, M. Wilson, M. C. Wilding, D. Daisenberger, M. Mezouar, and G. Neville Greaves, J. Phys.: Condens. Matter **19**, 415101 (2007).
[9] G. N. Greaves, M. C. Wilding, S. Fearn, D. Langstaff, F. Kargl, S. Cox, Q. V. Van, O. Majeérus, C. J. Benmore, R. Weber, C. M. Martin, and L. Hennet, Science **322**, 566 (2008).
[10] J. J. Z. Li, W. K. Rhim, C. P. Kim, K. Samwer, and W. L. Johnson, Acta Mater. **59**, 2166 (2011).
[11] S. Wei, F. Yang, J. Bednarcik, I. Kaban, O. Shuleshova, A. Meyer, and R. Busch, Nat. Commun. **4**, 2083 (2013).
[12] S. Krishnan, S. Ansell, J. J. Felten, K. J. Volin, and D. L. Price, Phys. Rev. Lett. **81**, 586 (1998).
[13] L. B. Skinner, C. J. Benmore, J. K. R. Weber, M. A. Williamson, A. Tamalonis, A. Hebden, T. Wiencek, O. L. G. Alderman, M. Guthrie, L. Leibowitz, and J. B. Parise, Science **346**, 984 (2014).
[14] G. Jacobs, I. Egry, K. Maier, D. Platzek, J. Reske, and R. Frahm, Rev. Sci. Instrum. **67**, 3683 (1996).
[15] C. Landron, X. Launay, J. C. Rifflet, P. Echegut, Y. Auger, D. Ruffier, J. P. Coutures, M. Lemonier, M. Gailhanou, M. Bessiere, D. Bazin, and H. Dexpert, Nucl. Instrum. Methods Phys. Res., Sect. B **124**, 627 (1997).
[16] S. Krishnan, J. J. Felten, J. E. Rix, J. K. R. Weber, P. C. Nordine, M. A. Beno, S. Ansell, and D. L. Price, Rev. Sci. Instrum. **68**, 3512 (1997).
[17] P.-F. Paradis, T. Ishikawa, J. Yu, and S. Yoda, Rev. Sci. Instrum. **72**, 2811 (2001).
[18] L. Hennet, D. Thiaudière, M. Gailhanou, C. Landron, J.-P. Coutures, and D. L. Price, Rev. Sci. Instrum. **73**, 124 (2002).
[19] L. Hennet, I. Pozdnyakova, A. Bytchkov, V. Cristiglio, P. Palleau, H. E. Fischer, G. J. Cuello, M. Johnson, P. Melin, D. Zanghi, S. Brassamin, J.-F. Brun, D. L. Price, and M.-L. Saboungi, Rev. Sci. Instrum. **77**, 053903 (2006).
[20] J. K. R. Weber, A. Tamalonis, C. J. Benmore, O. L. G. Alderman, S. Sendelbach, A. Hebden, and M. A. Williamson, Rev. Sci. Instrum. **87**, 073902 (2016).
[21] C. A. Rey, R. Sisler, D. R. Merkley, and T. J. Danley, Prog. Astronaut. Aeronaut. **127**, 270 (1990).
[22] D. Borosa, S. Kareth, and M. Petermann, Chem. Ing. Tech. **84**, 145 (2012).
[23] J. Magill, F. Capone, R. Beukers, P. Werner, and R. W. Ohse, High Temp. - High Pressures **19**, 461 (1987) , available at https://www.oldcitypublishing.com/journals/hthp-electronic-archive-home/hthp-electronic-archive-issue-contents/hthp-volume-19-number-5-1987/.
[24] R. W. Ohse, Int. J. Thermophys. **11**, 753 (1990).
[25] M. V. Kumar, J. T. Okada, T. Ishikawa, P.-F. Paradis, and Y. Watanabe, Meas. Sci. Technol. **25**, 085301 (2014).
[26] M. Nanko and K. Ishizaki, Proc. MRS Symp. **251**, 47 (1991).
[27] J. R. Rogers, R. W. Hyers, T. Rathz, L. Savage, and M. B. Robinson, AIP Conf. Proc. **552**, 332 (2001).
[28] N. H. El-Kaddah and D. G. C. Robertson, Metall. Trans. B **9**, 191 (1978).
[29] Ts. V. Rashev, R. I. Ivanov, and L. Saraiyanov, Zavod. Lab. **44**, 550 (1978).
[30] M. Chesswas, B. Cockayne, D. T. J. Hurle, E. Jakeman, and J. B. Mullin, J. Cryst. Growth **11**, 225 (1971).
[31] J. S. Haggerty, J. L. O'Brien, and J. F. Wenckus, J. Cryst. Growth **3–4**, 291 (1968).
[32] L. C. F. Blackman, P. H. Dundas, A. W. Moore, and A. R. Ubbelohde, Br. J. Appl. Phys. **12**, 377 (1961).
[33] H. J. Van Hook, Rev. Sci. Instrum. **36**, 1119 (1965).
[34] A. R. Bradshaw and D. Fort, Rev. Sci. Instrum. **63**, 5459 (1992).
[35] C. Ronchi, J. P. Hiernaut, R. Selfslag, and G. J. Hyland, Nucl. Sci. Eng. **113**, 1 (1993).
[36] S. Möhr and H. Müller-Buschbaum, Angew. Chem., Int. Ed. Engl. **34**, 634 (1995).
[37] S. Hosokawa and W.-C. Pilgrim, Rev. Sci. Instrum. **72**, 1721 (2001).
[38] D. Manara, C. Ronchi, and M. Sheindlin, Int. J. Thermophys. **23**, 1147 (2002).
[39] D. Manara, M. Sheindlin, W. Heinz, and C. Ronchi, Rev. Sci. Instrum. **79**, 113901 (2008).
[40] F. De Bruycker, K. Boboridis, R. J. M. Konings, M. Rini, R. Eloirdi, C. Guéneau, N. Dupin, and D. Manara, J. Nucl. Mater. **419**, 186 (2011).
[41] J. L. Schmehr, M. Aling, E. Zoghlin, and S. D. Wilson, Rev. Sci. Instrum. **90**, 043906 (2019).
[42] W. A. Phelan, J. Zahn, Z. Kennedy, and T. M. McQueen, J. Solid State Chem. **270**, 705 (2019).
[43] K. T. McDonald, Am. J. Phys. **68**, 388 (2000).
[44] T. Barois, G. Ricard, V. Champain, L. Gey, and H. Kellay, Phys. Fluids **32**, 045111 (2020).
[45] S. Davoust and L. Jacquin, *Sixth International Symposium on Turbulence and Shear Flow Phenomena* (Begell House, 2009), p. 1237.
[46] Q. Lin, W. R. Lindberg, D. L. Boyer, and H. J. S. Fernando, J. Fluid Mech. **240**, 315 (1992).